Int. J. Electrochem. Sci., 12 **(2017)** 6694 – 6704, doi: 10.20964/2017.07.36

International Journal of
ELECTROCHEMICAL
SCIENCE
www.electrochemsci.org

Development of an Ultrasensitive Electrochemical Method for Copeptin Content Determination

Yan Yang[1], *Songtao Gao*[1], *Jing Yang*[1], *Wei Yang*[1] *and Xiaoling Sun*[2,*]

[1] The Department of Cardiology, Heilongjiang Province Nangang Hospital, No.402 Guogeli St, Harbin, Heilongjiang, 150001 P.R. China
[2] The Clinical Laboratory of Digest, Heilongjiang Province Nangang Hospital, No.402 Guogeli St, Harbin, Heilongjiang, 150001 P.R. China
[*]E-mail: xiaolingsun58@qq.com

Received: 16 March 2017 / *Accepted:* 2 May 2017 / *Published:* 12 June 2017

Coronary heart disease, coronary syndrome and other cardiovascular diseases are globally predominant fatal conditions, although they can be prevented to a large extent. The determination of proper therapeutic options can be facilitated by copeptin level detection. A nanocomposite of reduced graphene oxide (RGO) and titania (TiO_2) was employed to fabricate a tag-free biosensor in this contribution. To specifically recognize and detect copeptin, this RGO-TiO_2 nanocomposite was functionalized with antibodies that are conjugated by protein (horseradish peroxidase). This biosensor exhibits enhanced biosensing traits for copeptin determination. Small-scale diagnostic equipment could be developed on the basis of this Ab-copeptin/RGO–TiO_2/ITO immunoelectrode.

Keywords: Cardiovascular diseases; Immunosensor; Copeptin; Graphene oxide; Titania

1. INTRODUCTION

Globally, cardiovascular diseases are primary fatal conditions, although they can be prevented to a large extent. Increased blood cholesterol concentration, namely, hypercholesterolemia, is among the top significant causes of increased cardiac arrest and cardiovascular disease occurrence, and thus, in clinical applications, it is essential to estimate blood cholesterol levels. It is clinically significant for patients with symptoms indicative of an acute coronary syndrome to be evaluated at an early stage. In these cases, possibly misguiding patient histories and/or electrocardiographic results can be increasingly complemented by biomarker determination. Since cardiac troponin can facilitate the therapeutic options and features convenient detection and myocardial tissue specificity, it is regarded as the exclusive marker and is normally employed in this case. However, it may also be useful for the

levels of copeptin and other markers specific to non-myocardial tissue to be determined. In 1972, Holwerda illustrated copeptin (arginine vasopressin (AVP)-associated glycopeptide) for the first time [1]. Containing a leucine-rich core segment, it is glycosylated and composed of 39 amino acids. A signal peptide (AVP), neurophysin II and copeptin make up preprovasopressin (a 164-amino acid precursor), from which copeptin is derived, similarly to AVP, and hence, copeptin is regarded as the C-terminal part of pro-AVP (CT-proAVP). For a long time, there has been no clear information about the physiologic function of copeptin, while AVP transfer (hypothalamus-neurohypophysis) is achieved by neurophysin II as a carrier protein. A possible prolactin-releasing factor role of copeptin was implicated by earlier studies [2], but this was later disproven [3]. In recent years, copeptin has been implied to help achieve the correct structural formation of the AVP precursor, as a basis for its effective proteolytic maturation [4]. It is most likely that an interaction between the calnexin–calreticulin system and copeptin occurs [5, 6]. Featuring protein-folding monitoring, this system interacts to a great extent with glycosylated proteins, leading to an increase in active hormone production and a decline in inactive hormone generation. Therefore, the pathogenesis of central diabetes insipidus can possibly be attributed to unproductive monomer folding without copeptin. Copeptin existing in a steadier oxytocin precursor is likely to be attributable to this supposition.

Two polyclonal antibodies to the amino acid sequence 132–164 of preprovasopressin are employed in the precursor's C-terminal domain, constituting a sandwich immunoluminometric assay for copeptin assessment that has been proposed in recent years [7]. Significant dynamics and precision are achieved by one antibody being tagged with acridinium ester for the determination of chemiluminescence, with the other bound to polystyrene tubes. This assay has remarkable potential to achieve mature AVP measurement.

The fields of food safety, environmental surveillance and global health are witnessing rising interest in point-of-care diagnostic equipment design with the improvements in nanotechnology and nanoscience in recent years [8]. The selective and sensitive determination of aptamers, PNA, smRNA, pathogens, *etc.* can be achieved by multifunctional nanomaterials [9, 10]. In terms of biosensor preparation, biomolecule or protein conjugation can be boosted by the existence of carboxyl, carbonyl, epoxide, hydroxyl and other accessible functional species on the basal edges/planes of a GO sheet [11-14].

RGO is prepared by tuning the electrical conductivity of GO with chemical reduction. High-speed heterogeneous electron shifts in RGO might be because its edge-plane-like defects are highly sensitive and it has extensive surface area, which lead to convenient functionalization with biomolecules, remarkable charge carrier mobility and boosted electrochemical traits in contrast to GO [15-23]. Furthermore, photodetectors, photovoltaics, field-effect transistors, biosensors and many other applications may be realized since RGO is mechanically flexible, inexpensive to synthesize and simple to prepare. Featuring non-toxicity, biocompatibility, low cost, strong oxidizing power and long-term stability, TiO_2 is regarded as another attractive material [24-26]. In addition, effective electron shift coordination between electrode and protein molecules as well as favored protein adsorption can be accomplished by TiO_2 nanoparticles. Many studies have examined the preparation of a TiO2 nanocomposite and RGO platform for electrochemical immunosensor fabrication. van der Waals interactions between the oxygen moieties and the graphene basal plane on the surface of TiO_2 might be

achieved by integrating RGO with TiO_2 via straight self-assembly. The electrochemical performance might be boosted because TiO_2 nanoparticles are uniformly distributed onto multilayered RGO. TiO_2 and RGO nanocomposite synthesis has been performed by Shen and co-workers.

To determine copeptin, we propose an electrochemical tag-free immunosensor in this work. The research results are presented herein. Horseradish peroxidase (HRP)-conjugated antibodies that are specific to copeptin are immobilized by the electrophoretic deposition of the prepared TiO_2–RGO composite onto a glass substrate that is coated with indium tin oxide (ITO). An extensive detection range and enhanced selectivity are realized through a desirably directed sensing platform offered by the HRP-conjugated antibodies on the TiO_2–RGO nanocomposite. To the best of our knowledge, this is the first time that an TiO_2–RGO composite has been employed for fabricating an electrochemical immunosensor for copeptin determination.

2. EXPERIMENTS

2.1. Chemicals

Sigma-Aldrich was the material source for *N*-hydroxysuccinimide (NHS), *N*-ethyl-*N*-(3-dimethylaminopropyl) carbodiimide (EDC), poly(diallyl dimethyl ammonium chloride) (PDDA, 20 wt.%), titanium butoxide, ascorbic acid and acetic acid. M/s Genetix Biotech, Asia Pvt. Ltd. (India) was the material source for copeptin, bovine serum albumin (BSA) and protein (HRP)-conjugated antibodies specific to copeptin. JCNANO, INC was the material source for the graphene oxide powder. All other reagents were of analytical grade and were employed without further purification. A solution of 0.1 M KH_2PO_4 and K_2HPO_4 was mixed to obtain a proper pH value to prepare phosphate buffer solution (PBS). All experiments were performed with 18.2 MΩ cm Milli-Q water.

2.2. Preparation of RGO-TiO_2 nanocomposite

A convenient hydrothermal technique was employed to prepare the TiO_2 nanoballs. First, a mixture of acetic acid (20 mL) with added titanium butoxide (2 mL) was stirred for 0.5 h and added to a Teflon-lined stainless steel autoclave (50 mL), followed by 10 h of oven heating at a temperature of 150 °C and natural cooling to ambient temperature. Centrifugation was used to collect the sediment, which was then washed. Subsequently, the TiO_2 nanoballs were generated as the product upon heating to 500 °C. The synthesis of the RGO-TiO_2 nanocomposite was achieved as follows. Sonication was used to disperse the TiO_2 nanoballs (100 mg) in water (20 mL), which was subsequently mixed with PDDA (2 mL) with stirring for 2 h. Centrifugation was used to collect the PDDA-functionalized TiO_2 with water washing, followed by its dispersion in water (20 mL) for an additional period. Subsequently, PDDA-functionalized TiO_2 was added to a GO dispersion (2 mL, 1 mg/mL). After being stirred for 1 h, the dispersion was mixed with ammonia solution (2 mL) and placed into a Teflon-lined stainless steel autoclave (50 mL), followed by 2 h of heating to 120 °C. Centrifugation was employed to collect the RGO-TiO_2 nanocomposite.

2.3. Characterization

An X-ray diffractometer (D8 Advance XRD, Bruker, Germany) with Cu Kα radiation was employed for the characterization of the crystal framework of as-prepared specimens. An Autolab potentiostat/galvanostat with a triple-electrode system (reference, auxiliary and working electrodes) in PBS (pH 7.0, 0.9% NaCl) containing 5 mM $[Fe(CN)_6]^{3-/4-}$ as the redox probe was used for the electrochemical analysis. The reference and auxiliary electrodes were Ag/AgCl (3 M KCl) and platinum wire, respectively. The surface functional species of the specimens were characterized via Fourier transform infrared spectrometry (FT-IR, PerkinElmer, and Spectrum BX II).

2.4. Biosensing platform fabrication

Prior to the covalent immobilization of antibodies (Ab-copeptin), the COOH group of the RGO/ITO electrode was activated using EDC as the coupling agent and NHS as the activator. A 1 ng/mL antibody solution was freshly prepared in phosphate buffer (PBS, pH 7.4). Ten microliters of this solution was uniformly spread on the EDC/NHS-activated RGO-TiO_2/ITO electrode surface, which was then incubated in a humid chamber for approximately 4 h at room temperature. A significant amide (CO–NH) bond could be yielded between the amine species of HRP-conjugated Ab-copeptin and the carboxyl species of RGO via covalent interaction. Furthermore, this interaction could be boosted by HRP, which naturally interacts with TiO_2 nanoparticles and RGO in an electrostatic fashion. The as-prepared immunoelectrode was rinsed with PB (pH 7.0) to remove free Ab-copeptin. To block non-specific sites, this Ab-copeptin/RGO-TiO_2/ITO immunoelectrode was treated with a 1 mg/mL BSA solution for approximately 4 h. The terminal BSA/Ab-copeptin/RGO–TiO_2/ITO immunoelectrode product was stored at 4 ℃ storage when not in use.

3. RESULTS AND DISCUSSION

RGO and RGO-TiO_2 are characterized via XRD (Figure 1). Since the interlayer distance becomes narrower and the RGO sheets are packed more tightly after the GO oxide species and intercalated water molecules are removed, GO reduction occurs, as revealed by the (002) reflection plane coinciding with the wide and predominant 23.5° (3.41 Å) peak [27]. TiO_2 anatase phase is revealed by diffraction from the (101) and (200) planes coinciding with the 2θ = 24.8° and 48.2° peaks, which are significant in terms of the RGO–TiO_2 nanohybrid. That anatase phase is present in the TiO_2 is indicated by the (204), (211), (004) and (105) (JCPDS 894921) diffraction planes. The whole set of TiO_2-related peaks are observed for the TiO_2 nanoparticles. Nevertheless, the separation of the monitored RGO layers with the nanoparticle spacers and the absence of stacking are revealed by the (101) peak coinciding with an insignificant peak shown by the (200) diffraction plane in the RGO–TiO_2 composite, indicating that the observed RGO layers are separated by nanoparticles acting as spacers and are not stacked together [28]. A disordered framework of the graphene sheets is denoted by the absence of obvious graphite-related diffraction peaks.

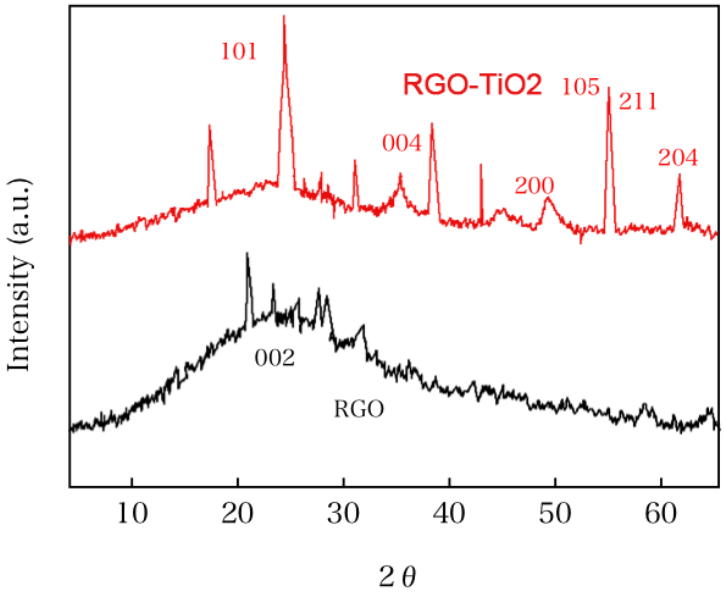

Figure 1. Powder X-ray diffraction profiles of RGO and RGO–TiO_2.

As indicated in Figure 2A, RGO-TiO_2 nanohybrid and RGO synthesis was verified via Raman spectroscopy studies. The atoms of carbon vibrate with the sp^3 electronic configuration of disordered graphene, and thus, a D band occurs, as revealed by the 1345 cm^{-1} absorption peak in the inset. The in-plane vibration of the sp^2-bonded carbon atoms is related to the G band-linked 1585 cm^{-1} peak. The peaks associated with the anatase phase E_g (634 cm^{-1}), A_{1g} (511 cm^{-1}) and B_{1g} (397 cm^{-1}) modes in the low-frequency domain are revealed in the Raman spectrum for RGO-TiO_2. As indicated in the inset, in contrast to RGO, RGO-TiO_2 exhibits lowered intensity in the D band (1347 cm^{-1}). That the RGO-TiO_2 nanohybrid is formed is revealed by an insignificant lower shift in wavenumber. Since the average size of the sp^2 region increases and defects are present in the RGO, the D/G intensity ratio of RGO-TiO_2 is as low as 0.94 in contrast to the 1.31 obtained for RGO. After GO is reduced, there is an increase in graphene sheet defects, as denoted by a decreased D/G intensity ratio of the GO sheets.

The 577 cm^{-1} peak reflecting absorption corresponding to Ti–O bonding is observed for the RGO–TiO_2/ITO film, as indicated in its FT-IR spectra in Figure 3. The C–H stretching vibration on the surface of the nanocomposite is reflected by the 959 cm^{-1} peak. That GO sheets are present in the RGO–TiO_2/ITO film is revealed by 1748 cm^{-1}, 1661 cm^{-1}, 1221 cm^{-1} and 1050 cm^{-1} peaks. The C=O stretching vibrations of COOH species were reflected by the first peak [29], C=C aromatic vibrations by the second, and C–O stretching vibrations by the last two.

UV-Vis studies were conducted on the ant-TiO_2 and RGO–ant-TiO_2 from 200 to 700 nm. The absorption peak found at 265 nm is due to the quantum confinement effect of the ant-TiO_2. The direct band gap (*E*g) of ant-TiO_2 was estimated to be 3.8 eV, which is higher than that of the bulk material. It can be seen that distinct peaks appear at 334 nm and 250 nm, corresponding to the π–π* transition of the aromatic C–C bonds of RGO modified with ant-TiO_2 [30, 31].

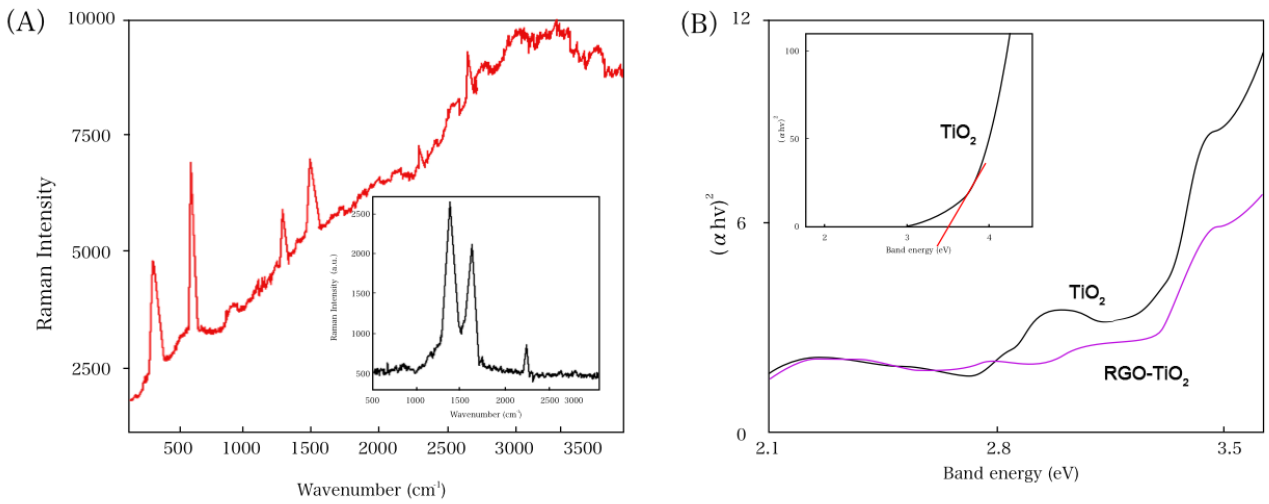

Figure 2. (A) Raman spectra of the RGO-TiO_2 nanohybrid and Raman spectra of RGO (inset) and (B) the plot of $(\alpha hv)^2$ vs. band energy (eV).

The vibrations in non-oxidized graphitic regions account for the intensive peaks in the vicinity of the 1598 cm^{-1} peak. After BSA and Ab-copeptin are immobilized, amide bonds can form, thus increasing the intensity of the 1598 cm^{-1} peak. Since Ab-copeptin and then BSA are incorporated onto the RGO–TiO_2/ITO nanohybrid surface, there is a peak transfer in the fingerprint domain ranging from 500 to 600 cm^{-1}. The surface functionalization by BSA and Ab-copeptin is indicated by extra peaks, namely, the 3199, 2027 and 1045 cm^{-1} peaks.

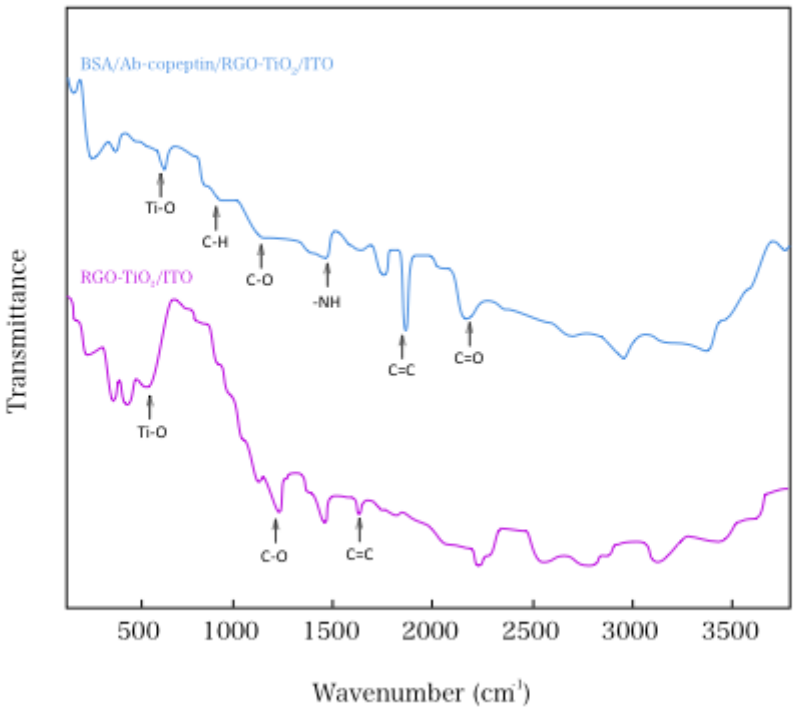

Figure 3. FT-IR spectra of the RGO-TiO_2/ITO nanohybrid and the BSA/Ab-copeptin/RGO-TiO_2/ITO immunoelectrode.

As indicated in Figure 4, the original ITO electrode, RGO–TiO_2/ITO nanohybrid, Ab-copeptin/RGO–TiO_2/ITO immunoelectrode and BSA/Ab-copeptin/RGO-TiO_2/ITO immunoelectrode were characterized in PBS containing 5 mM $[Fe(CN)_6]^{3-/4-}$ via cyclic voltammetry (CV) profiles at a scan rate of 20 mV/s. Since the electrons are transported at a high speed between the electrolyte and electrode, the oxidation current for RGO–TiO_2/ITO electrode shifts to a more elevated potential in contrast to the original ITO, with an approximately 4-fold rise in the current magnitude of the former. This may be attributed to the heterogeneous electron transfer in the graphene sheet and oxygen-containing groups at the edges of the graphene sheets. Additionally, the excellent electrocatalytic ability of the TiO_2 embedded in the RGO results in faster electron transfer between the electrode and electrolyte. The protein molecules' insulating nature causes a decline in current with an insignificant shift to a lower potential, where the electron flow declined, which was attributed to the functionalization of the RGO–TiO_2/ITO electrode by the Ab-copeptin that was conjugated with the macromolecular protein. The current magnitude declines due to the impeded electron shift between the electrode and the medium, because the Ab-copeptin/RGO–TiO_2/ITO electrode was modified by BSA, which is insulating.

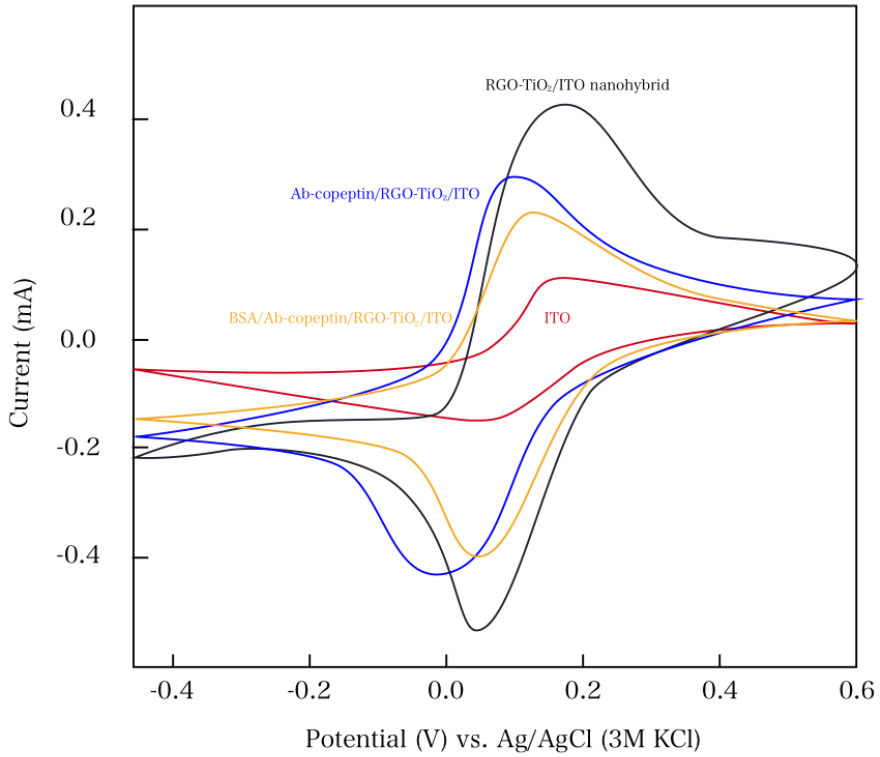

Figure 4. CV spectra of ITO, RGO-TiO_2/ITO nanohybrid, Ab-copeptin/RGO-TiO_2/ITO immunoelectrode and BSA/Ab-copeptin/RGO-TiO_2/ITO bioelectrode.

Amperometric immunosensors are commonly fabricated for target molecule determination. However, in a label-free immunoassay process, amperometric immunosensors are not suitable for the detection of non-active immunocomplexes. EIS can monitor the target substance directly without

labeling, and thus, it is expected that a direct immunosensor analysis method can be developed based on EIS. The impedance values of the BSA/Ab-copeptin/RGO–TiO_2/ITO were recorded at different concentrations of copeptin [32]. As indicated in Figure 5, the BSA/Ab-copeptin/RGO–TiO_2/ITO immunoelectrode was characterized via its impedimetric response as a function of copeptin concentration (10–500 ng/mL) with 5 min incubation in PBS containing $[Fe(CN)_6]^{3-/4-}$. As the concentration of copeptin rises, the capacitance declines, possibly because of variation of the dielectric/blocking traits of the electrolyte–electrode interface caused by the interaction between the antigen and antibody. Since Ab-copeptin interacts with copeptin, it is predictable that the capacitance would decline because of the increased electrolyte–electrode distance. Furthermore, because a decreasing number of polar copeptin protein molecules substitute water molecules on the surface of the electrode, the capacitance decline results from copeptin and Ab-copeptin interaction. The plotted variation in capacitance *vs.* the analyte (antigen) concentration could be employed for the calibration of the capacitive immunosensor, with 10–500 ng/mL obtained as the linear relationship range. In similar circumstances, the capacitance variation as a function of copeptin concentration was also recorded for the BSA/Ab-copeptin/RGO–TiO_2/ITO immunoelectrode. The obtained linear regression coefficient (r^2) was 0.989 for the BSA/Ab-copeptin/RGO–TiO_2/ITO immunosensor. Possibly since the nanocomposite of RGO–TiO_2 possesses extended surface area and functional traits, the as-prepared biosensor is more sensitive. Enhanced biosensor efficiency might be attributed to the rise in loading capacity for antibody molecules possibly induced by the existence of available functional species on the RGO–TiO_2. Through calculation via $3\sigma_b/m$ criteria, 0.148 ng/mL is obtained as the detection value (lower) for the as-prepared immunosensor. The sensing performance of the proposed sensor was compared with recently reported sensors, as shown in Table 1.

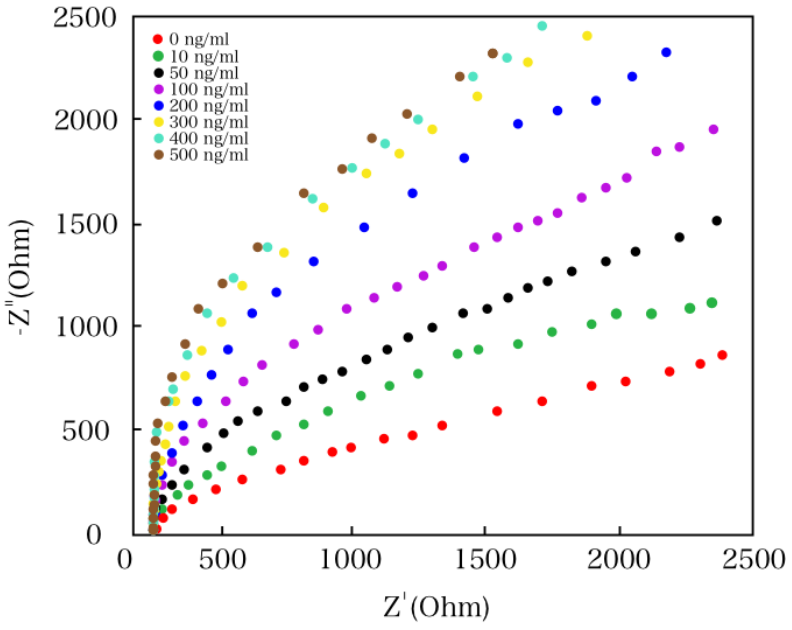

Figure 5. Electrochemical impedance response studies of the BSA/Ab-copeptin/RGO–TiO_2/ITO immunoelectrode as a function of copeptin concentration (10–450 ng/mL).

Table 1. Performance comparison of the BSA/Ab-copeptin/RGO–TiO_2/ITO and other copeptin determination methods.

Method	Linear range	Detection limit	Reference
Enzyme-linked immunosorbent assay	15-500 ng/mL	1.4 ng/mL	[33]
ELISA	40-200 ng/mL	10 ng/mL	[34]
ELISA	17-400 ng/mL	—	[35]
Elecsys® troponin T high-sensitive system	—	14 pg/mL	[36]
BSA/Ab-copeptin/RGO–TiO_2/ITO	10–500 ng/mL	0.148 ng/mL	This work

The specificity of the BSA/Ab-copeptin/RGO–TiO_2/ITO immunoelectrode was tested with 300 ng/mL copeptin, 5 mM ascorbic acid, 5 mM uric acid and 5 mM glucose. The immunoelectrode was incubated with the above pathogens and metabolites (15 μL). As indicated in Figure 6, after the immunoelectrode was mixed with the above pathogens, no obvious electrochemical response variation was monitored in the assessments. Moreover, the effects of trace levels of metal ions (1 μM) such as Zn^{2+}, Cu^{2+}, Hg^{2+} and Cd^{2+} were also investigated, with less than a 5% change of impedance value recorded, revealing the probe's specificity to copeptin.

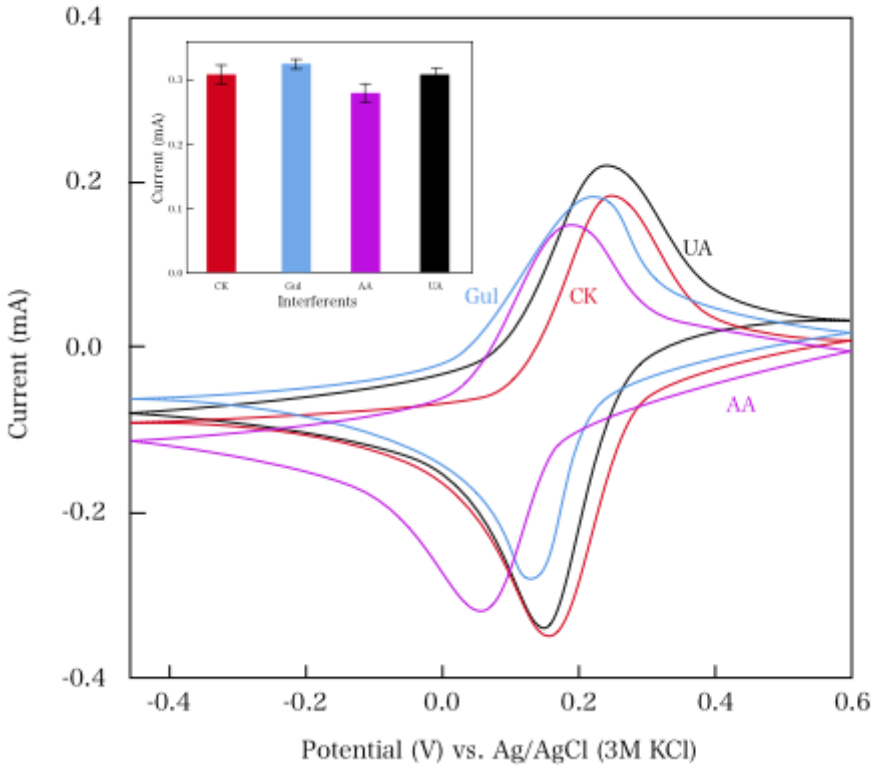

Figure 6. Interference studies of BSA/Ab-copeptin/RGO–TiO_2/ITO immunoelectrode with glucose (Glu), ascorbic acid (AA) and uric acid (UA); the histogram plot with all interferents indicated in the inset.

Ten successive CV sweeps between 0.0 and 0.5 V at 50 mV/s in a buffer of $NH_3 \cdot H_2O$–NH_4Cl (0.1 M, pH 9.3) were used to remove any adsorbents after each detection. Copeptin (300 ng/mL) was tested with multiple electrodes to investigate the reproducibility of the immunoelectrode, where the

current magnitude variations were monitored. Desirable precision was revealed by no obvious current value variation, as seen in Figure 7A. As indicated in Figure 7B, CV profiles at 10-day intervals over approximately 30 days were used to characterize the immunoelectrode storage stability. For as long as 30 days, no clear variation in current was observed, followed by a 4% current variation from to the primary current value. Therefore, for as long as 30 days, excellent storage stability can be obtained for BSA/Ab-copeptin/RGO–TiO_2/ITO immunoelectrodes.

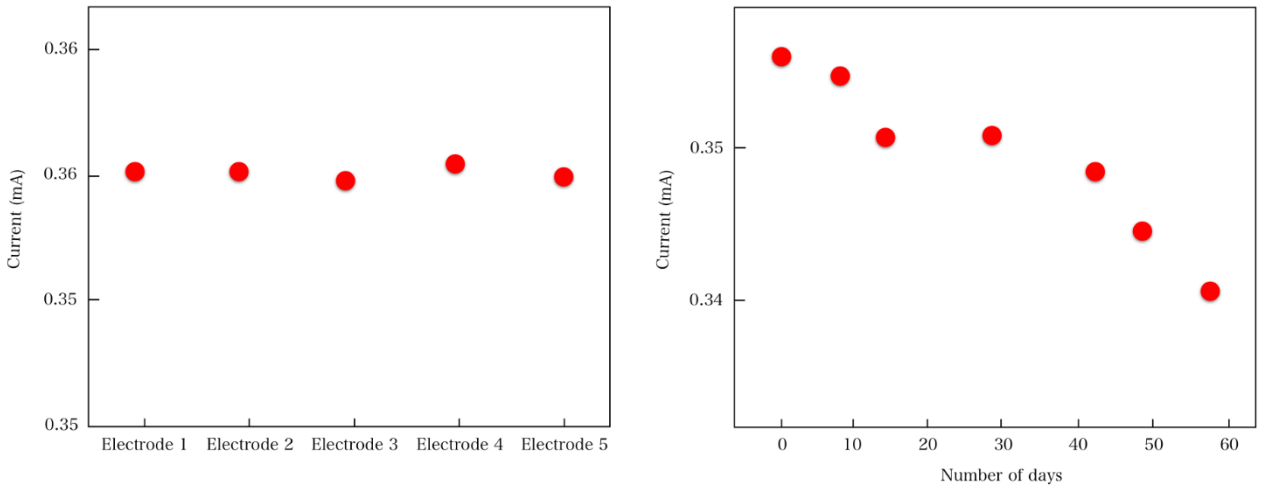

Figure 7. (A) Reproducibility study of the BSA/Ab-copeptin/RGO–TiO_2/ITO immunoelectrode with copeptin (300 ng/mL). (B) The stability profile of the BSA/Ab-copeptin/RGO–TiO_2/ITO immunoelectrode (300 ng/mL) over 30 days.

4. CONCLUSION

Copeptin detection on the basis of interactions between its antibody and antigen was achieved by fabricating the RGO-TiO_2 nanohybrid-based tag-free immunosensor discussed in this contribution. The sensor is stable for a long period and is significantly sensitive, with a desirably low limit of detection, as indicated in the studies concerning the electrochemical response of the BSA/Ab-copeptin/RGO–TiO_2/ITO immunoelectrode as a function of copeptin concentration. The RGO–TiO_2-based immunosensor can feasibly be applied in medical diagnosis due to its remarkable sensing (supercapacitive) behavior.

ACKNOWLEDGEMENT
This work was supported by research project of National Health and Family Planning Commision of Heilongjiang Province (2016-500).

References

1. D. Holwerda, *European Journal of Biochemistry*, 28 (1972) 340.
2. G. Nagy, J. Mulchahey, D. Smyth and J. Neill, *Biochemical and Biophysical Research Communications*, 151 (1988) 524.
3. J. Hyde, W. North and N. Ben-Jonathan, *Endocrinology*, 125 (1989) 35.
4. C. Barat, L. Simpson and E. Breslow, *Biochemistry*, 43 (2004) 8191.

5. A. Parodi, *Annual Review of Biochemistry*, 69 (2000) 69.
6. J. Schrag, D. Procopio, M. Cygler, D. Thomas and J.M. Bergeron, *Trends in Biochemical Sciences*, 28 (2003) 49.
7. N. Morgenthaler, J. Struck, C. Alonso and A. Bergmann, *Clinical Chemistry*, 52 (2006) 112.
8. A. Turner, *Chemical Society Reviews*, 42 (2013) 3184.
9. N. Gilmartin and R. O'Kennedy, *Enzyme and Microbial Technology*, 50 (2012) 87.
10. P. Ray, S. Khan, A. Singh, D. Senapati and Z. Fan, *Chemical Society Reviews*, 41 (2012) 3193.
11. W. Yang, K. Ratinac, S. Ringer, P. Thordarson, J. Gooding and F. Braet, *Angewandte Chemie International Edition*, 49 (2010) 2114.
12. Y. Shao, J. Wang, H. Wu, J. Liu, I.A. Aksay and Y. Lin, *Electroanalysis*, 22 (2010) 1027.
13. Z. Zhuang, J. Li, R. Xu and D. Xiao, *International Journal of Electrochemical Sci*ence 6 (2011) 2149.
14. M. Lyons, A. Cakara, P. O'Brien, I. Godwin and R. Doyle, *International Journal of Electrochemical Science*, 7 (2012) 768.
15. Z. Yao, X. Yang, F. Wu, W. Wu and F. Wu, *Microchimica Acta*, 183 (2016) 2799.
16. H. Bagheri, A. Hajian, M. Rezaei and A. Shirzadmehr, *Journal of Hazard Material*, 324 (2017) 762.
17. E. Asadian, S. Shahrokhian, A. Zad and F. Ghorbani-Bidkorbeh, *Sensors and Actuators B: Chemical*, 239 (2017) 617.
18. V. Gupta, R. Goyal and R. Sharma, *Talanta*, 76 (2008) 859.
19. V. Gupta, N. Mergu, L. Kumawat and A. Singh, *Sensors and Actuators B: Chemical*, 207 (2015) 216.
20. V. Gupta, N. Mergu, L. Kumawat and A. Singh, *Talanta*, 144 (2015) 80.
21. V. Gupta, A. Singh and L. Kumawat, *Sensors and Actuators B: Chemical*, 195 (2014) 98.
22. S. Srivastava, V. Gupta and S. Jain, *Analytical Chemistry*, 68 (1996) 1272.
23. V. Gupta, L. Singh, R. Singh, N. Upadhyay, S. Kaur and B. Sethi, *Journal of Molecular Liquids*, 174 (2012) 11.
24. X Zhang, H. Li, X. Cui and Y. Lin, *Journal of Materials Chemistry*, 20 (2010) 2801.
25. H. Khani, M. Rofouei, P. Arab, V. Gupta and Z. Vafaei, *Journal Hazard Material*, 183 (2010) 402.
26. V. Gupta, H. Karimi-Maleh and R. Sadegh, *International Journal of Electrochemical Science*, 10 (2015) 303.
27. J. Shen, M. Shi, B. Yan, H. Ma, N. Li and M. Ye, *Nano Research*, 4 (2011) 795.
28. C. Nethravathi and M. Rajamathi, *Carbon*, 46 (2008) 1994.
29. M. Xing, B. Qiu, X. Li and J. Zhang, TiO_2/Graphene Composites with Excellent Performance in Photocatalysis, Nanostructured Photocatalysts, Springer2016, pp. 23.
30. X. Li, F. Chen, C. Lian, S. Zheng, Q. Hu, S. Duo, W. Li and C. Hu, *Journal of Cluster Science*, 27 (2016) 1877.
31. C. Zhou, X. Wang, X. Kuang and S. Xu, *Journal of Micromechanics and Microengineering*, 26 (2016) 075003.
32. G. Lewis Jr, G. Lewis Sr and W. Olbricht, *Measurement Science and Technology*, 19 (2008) 105102.
33. X. Zhu, J. Chen, F. Zhou, Q. Liu, G. Chen and J. Zhang, *Critical Care*, 15 (2011) R288.
34. X. Yang, Z. Zhigang and C. Sanbao, *Journal of Radioimmunology*, 2 (2008) 001.
35. F. Purroy, I. Suárez-Luis, S. Cambray, J. Farré, I. Benabdelhak, G. Mauri-Capdevila, J. Sanahuja, A. Quílez, R. Begué and M. Gil, *Acta Neurologica Scandinavica*, (2015)
36. U. Lotze, H. Lemm, A. Heyer and K. Müller, *Vasc Health Risk Manag*, 7 (2011) 509.